Mechatronics 30 (2015) 327–337

Contents lists available at ScienceDirect

Mechatronics

journal homepage: www.elsevier.com/locate/mechatronics

Terminal sliding mode control of automated car-following system without reliance on longitudinal acceleration information

Shengbo Eben Li [a], Kun Deng [b], Keqiang Li [a], Changsun Ahn [c,*]

[a] State Key Lab of Automotive Safety and Energy, Dept. of Automotive Eng., Tsinghua University, Beijing 100084, China
[b] Coordinated Science Laboratory, University of Illinois at Urbana-Champaign, Urbana, IL 61801, USA
[c] School of Mechanical Engineering, Pusan National University, Busan 609-735, Republic of Korea

ARTICLE INFO

Article history:
Received 9 March 2014
Revised 21 August 2014
Accepted 28 September 2014
Available online 25 October 2014

Keywords:
Vehicle automation
Minimum sensor framework
Car-following
Sliding mode control

ABSTRACT

The framework of minimum sensor helps reduce the number of sensors in vehicle automation. This framework is a promising approach to decrease hardware costs of driverless vehicles without significantly losing desirable performance and reliability. Even though cost is not the concern, it also provides a straightforward fault-tolerant solution in case of sensor failures. This paper presents a terminal sliding mode (TSM) controller for automated car-following systems, where only the radar is additionally equipped and no acceleration information is used. The automated controller design is based on the so-called finite-time convergence concept after compensating for the nonlinearities of powertrain dynamics via an inverse model. The controller uses a terminal function with non-integer exponents to improve the convergence rate of sliding mode, and designs a matched terminal attractor as the reaching law outside of sliding mode. The newly designed TSM controller has high robustness to modeling uncertainties and external disturbances, without the issues of singularity and chattering that are usually accompanied with conventional counterparties. For nominal conditions, it is proved that the inter-vehicle state from any initial position asymptotically converges to zero. For uncertain conditions, the bounded closed-loop stability is guaranteed under some mild assumptions on preceding vehicle acceleration and road slope. The effectiveness of this controller is validated using computer simulations and road tests on a passenger car equipped with an internal combustion engine and 5-speed automatic transmission.

1. Introduction

An autonomous vehicle is capable of fulfilling the driving capabilities of humans with a traditional car. Besides recognizing route and sensing environment, automated motion control is the most important issue for driverless automation. The automation techniques have been successfully developed and utilized to control some aspects of vehicle dynamics [1–4]. Some elementary demos date back to the 1980s. Since then, numerous major companies and research organizations have developed prototyping autonomous vehicles, and significant advances have been made in technology. In spite of the various benefits to increased vehicle automation, some foreseeable challenges persist, including cost of hardware, liability for damage, cyber security, human–machine co-pilot, implementation of legal framework, establishment of government regulations, etc. Therefore, it is commonly believed that fully vehicular automation is still not implementable in the near future, and semi-automation will be the dominating status for a long time. As the continuum of cruising control and adaptive cruise control, longitudinal automation is one of the most significant technologies for semi-automation.

In a commercial product, the use of an automated driving system is often quite expensive due to the cost of supplementary sensors, e.g. radars and IMUs (Inertial Measurement Unit), and actuators, e.g. electric–hydraulic braking (EHB) system [5]. The concept of minimum sensor control, aiming to reduce the number of sensors, is promising to reduce the hardware cost further. Under this framework, autonomous vehicles are only equipped with radar sensors to detect the distance between the preceding and following vehicles, which is the major requisite for inter-vehicle range detection, however IMUs are not equipped. The longitudinal controller is then implemented only based on outputs of radar, but without reliance on any vehicle acceleration information. This approach can directly reduce the cost of longitudinal automation of vehicles. Even though cost is not important in some special cases, e.g. military applications, it still provides a straightforward

* Corresponding author.
E-mail addresses: lisb04@gmail.com (S.E. Li), kundeng2@illinois.edu (K. Deng), likq@tsinghua.edu.cn (K. Li), sunahn@pusan.ac.kr (C. Ahn).

http://dx.doi.org/10.1016/j.mechatronics.2014.09.014
0957-4158/

fault-tolerant solution in the case of acceleration sensor failures [6]. Basic strategies for vehicle longitudinal automation can be categorized into two types, i.e., hierarchical control [7,8] and integrated control [10,11]. In the first one, an upper layer controller and a lower layer controller are designed separately, and an interim control variable (often being desired longitudinal acceleration) connects the two controllers together. In the second one, only an integrated controller is synthesized between the inputs (vehicle states) and the outputs (actuator commands) of the plant. In the minimum sensor framework that the longitudinal acceleration measurement is not accessible, the hierarchical control strategy is not applicable. An immediate remedy for this issue is to estimate the acceleration using other measurements, for example, wheel speeds and/or GPS. The pioneering work of Hebbale and Ghoneim [12] shed light on estimating acceleration from wheel speed based on the Kalman filter. Ferrara and Pisu [6] designed a model-based observer that considers the nonlinearities of vehicle longitudinal dynamics. However, these approaches may cause large estimation error on acceleration due to tire slip, sensor noise, powertrain uncertainties, and external disturbances (e.g., road slop and environmental wind), thus leading to large error in acceleration control and further large error on controlling inter-vehicle states.

This paper proposes an alternative approach for the automated car-following system that does not depend on estimated acceleration. The challenges without the reliance on acceleration information are the performance deterioration in the convergence rate and the closed-loop stability. To address this issue, we consider a recent advance on sliding mode control method, i.e. terminal sliding mode (TSM). The TSM uses so-called the finite-time convergence concept, and has been proven to have special merits on high stability and robustness to modeling uncertainties and external disturbances. This advantage comes from its extraordinary terminal function. To the best of our knowledge, Venkataraman and Gulati (1993) are the first researchers to introduce terminal function to sliding mode control field [13]. Considering a second-order robotic system, an earlier terminal function (TF) is selected as $s = \dot{x} + \alpha x^{p/q}$, where $x \in \mathbb{R}$ is the system state, $\alpha \in \mathbb{R}^+$ and $p, q \in N$, satisfying $p < q$. It is well known that a linear sliding function generates exponential stability, and the state infinitely approaches, but is never exactly equal to, the equilibrium point. On the contrary, the terminal function enables a finite time convergence property because of the non-integer exponent. For multi-input multi-output (MIMO) systems, Man and Yu (1996) extended this type of terminal function to high-dimensional situations [14]. The following research also proved its finite time convergence property for some cascading systems [15]. This control method was applied to n-link rigid robotic manipulators and its good robustness to large uncertain dynamics was also observed [16]. Compared to a linear sliding function, earlier terminal function might have slower convergence speed although it still converges in finite time. The reason is as follows: since $p < q$, the exponent of state x is smaller than one. Thus, when $x \gg 1$, the derivative $\dot{x}$ in the sliding mode will be much smaller than that in similar linear sliding mode. To address this issue, Yu and Man et al. (1997) proposed a terminal function with fast convergence characteristics [17], called fast terminal function (FTF) with $s = \dot{x} + \alpha x^{\gamma} + \alpha x^{\rho}$, where $0 < \gamma < 1$, $\rho > 1$, $\gamma, \rho, \in \mathbb{R}^+$. The FTF contains a polynomial term of order higher than 1, forcing state to converge faster than any linear sliding function. Yu and Guo et al. (2006) obtained its global description and applied it to design both reaching law and sliding function [18].

One major drawback of TSM control is the singularity issue. Yu and Man et al. (1997) modified the high-order FTF and pointed out that the singularity disappears if some exponents satisfy an inequality condition [17]. In [19,20], researchers designed a terminal sliding mode control law for a nonlinear dynamic system. However, for actual plants, the instantaneous singularity still exists because of parameter perturbations, external disturbances, and measurement errors. Feng and Bao et al. (2002) developed a nonsingular terminal function (NTF), realizing that the state converges in finite time during the sliding mode and the control law has no negative exponential term [21], shown as $s = \beta \dot{x}^{p/q} + x$, where $p > 0$, $q > 0$, q is integer, and $1 < p/q < 2$. Combined with the global reaching conditions, a nonsingular terminal sliding mode (NTSM) control law can be designed in [22,23]. But this kind of terminal function has slow convergence speed in the region far away from equilibrium point. Moreover, a switching term inevitably exists in the control law, causing the commonly known as chattering problem (another famous issue in sliding mode control). This largely limits its application in engineering practice.

The objective of this paper is to design an automated car-following controller that does not rely on the information of longitudinal acceleration. To maintain desirable robustness, the terminal sliding model control method is adopted for controller design, in which the rapidity and singularity are the two key concerns. A fast and nonlinear terminal function with non-integer exponent is proposed to improve the convergence rate of the sliding mode, and a matched terminal attractor with negative exponent is designed as the reaching law outside of the sliding mode. The designed controller has high robustness to model uncertainties and external disturbances, without the issues of singularity and chattering that often company with many other conventional sliding mode controllers. For both nominal conditions and uncertain conditions, the stability and robustness are analyzed and proved. The remainder of this paper is structured as follows: Section 2 summarizes the fundamentals of the nonsingular fast terminal sliding mode (NFTSM) control method. In Section 3, the car-following system method is introduced and modeled. The design of longitudinal controller is presented in Sections 4 and 5 analyzes the stability and robustness of closed loop system for both nominal and uncertain conditions. In Section 6, the effectiveness of this newly proposed control method is studied through both computer simulations and field tests.

2. Modeling of automated car-following system for control

A typical automated car following system includes two vehicles: one preceding vehicle (PV) and one following vehicle (FV). The predecessor is the closest vehicle located in the same lane as the follower. Here, the follower is a passenger car, only equipped with front-viewed millimeter wave (MMW) radar, but without any IMUs (i.e. no acceleration information is accessible). The outputs of MMW radar include inter-vehicle distance d and relative speed. Δv Other information of vehicle longitudinal information will be acquired via original CAN bus, which reduces the cost of equipping the car with new sensors and signal processing system. Fig. 1 shows a typical automated car-following system, running on a slope.

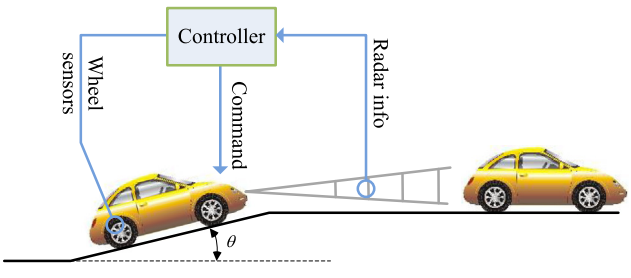

Fig. 1. Automated car-following system.

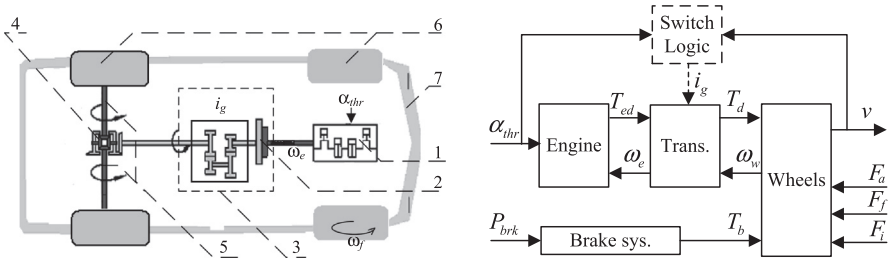

1-Engine, 2-torque converter, 3-automatic transmission, 4-differential and final gear, 5-rear half-shaft, 6-wheels, 7-body

Fig. 2. Sketch of vehicle powertrain dynamics.

Fig. 2 sketches the longitudinal dynamics of the FV. Its major components include a gasoline engine, a 5-gear automatic transmission (including torque converter), a differential, a final gear, two rear half-shafts, four wheels, and a vehicle body [8,9]. The necessary signals for control include engine speed ω_e, vehicle speed v, gear ratio of automatic transmission i_g, inter-vehicle distance d, and relative speed Δd. They are all measurable under the current sensing framework. The control input is the throttle angle α_{thr}. The powertrain is controlled by an electronic throttle device, instead of a human driver, to automatically adjust vehicle longitudinal motion. Here, we do not consider controlling the braking system (see Fig. 3).

To accurately describe the longitudinal dynamics, Cho and Hedrick [24] have suggested using a model with 8 states and 2 time-delays. However, for any embedded control systems using sliding mode control [2], adaptive control [5], or model predictive control [25], a lower order vehicle model is more desirable in order to simplify the design task and facilitate the real-time application. Here, we only consider major longitudinal dynamics of vehicle body and neglect all secondary dynamics, e.g., fuel delivery and combustion, rear shaft torsion, wheel slipping dynamics, etc. [26]. The simplified model for vehicle longitudinal dynamics is described below:

$$\begin{aligned} &T_e = \mathrm{MAP}(\omega_e, \alpha_{thr}) \\ &T_{ed} = \tfrac{1}{\tau_e s+1} T_e, \quad T_{ed} - T_p = J_e \dot{\omega}_e \end{aligned} \tag{1}$$

$$\begin{aligned} &T_p = C_{TC}\omega_e^2, \quad T_t = K_{TC} T_p \\ &\tfrac{i_g i_0 \eta_T T_t}{r_w} = \delta M \dot{v} + \tfrac{1}{2} C_A A \rho v^2 + M g_m f + M g_m \theta \end{aligned}$$

where T_e is the engine torque command, T_{ed} is the actual engine torque, τ_e is the time constant of engine dynamics, $\mathrm{MAP}(\cdot,\cdot)$ is a nonlinear tabular function representing engine static characteristics, T_p is the pump torque of torque converter, J_e is the inertia of fly wheel, T_t is the turbine torque of torque converter, C_{TC} is the capacity coefficient of torque converter, K_{TC} is the torque ratio of torque converter, i_0 is the ratio of final gear, η_T is the mechanical efficiency of driveline, r_w is the rolling radius of wheels, M is the vehicle mass, v is the vehicle speed, C_A is the coefficient of aerodynamic drag, A is the frontal cross-area, ρ is the air density, g_m is the gravity coefficient, f is the coefficient of rolling resistance, θ is the road slope, and δ is the lumping coefficient, defined as

$$\delta = 1 + \frac{I_w}{M \cdot r_w^2} \tag{2}$$

where I_w is the inertial moment of four wheels.

Note that i_g is discontinuous, which is determined by throttle angle α_{thr} and vehicle speed; C_{TC} and K_{TC} are not constant, varying with the speed ratio of torque converter:

$$\begin{aligned} &i_g = i_g(\alpha_{thr}, v) \\ &C_{TC} = C_{TC}(\lambda), \quad K_{TC} = K_{TC}(\lambda) \\ &\lambda = \frac{\omega_e}{\omega_t}, \quad \omega_t = i_g i_0 \frac{v}{r_w} \end{aligned} \tag{3}$$

where $i_g(\alpha_{thr}, v)$ is shown in Fig. 4, $C_{TC}(\lambda)$ and $K_{TC}(\lambda)$ are shown in Fig. 5, and λ is the speed ratio of torque converter, ω_t is the turbine speed of torque converter. Other vehicle parameters are summarized in Table 1. The simplified model for control is validated by field tests of a passenger car. The setup of the passenger car is further introduced in Section 5. The car experiment is carried out on a flat and long road, with maximum road slope <2%, and wind speed <8 m/s. The mass of experimental car includes driver, experimenter, and equipped devices, etc. The signals of throttle angle, engine speed, vehicle speed, vehicle acceleration are collected at the frequency of 10 Hz. Fig. 6 illustrates the validation results of the simplified vehicle model.

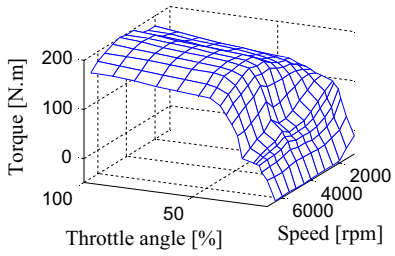

Fig. 3. Engine static characteristics (MAP function).

3. Synthesis of automated car-following controller

Autonomous and semi-autonomous road vehicles have been created for transporting passengers and cargo. A widely known application is the adaptive cruise control, which is an enhancement of traditional cruise control system for road vehicles that automatically adjusts the vehicle speed to maintain a safe distance from vehicles ahead. Under the minimum sensor framework, the automated car-following system has no acceleration information and thus the hierarchical control strategy is not applicable for controller design. For the sake of controller design, a two-state space model including both vehicle and inter-vehicle longitudinal dynamics is derived in order to use the integrating control strategy. Define two state variables as relative speed Δv and distance error Δd

$$\begin{aligned} &\Delta v = v_p - v \\ &\Delta d = d - d_{des} \\ &d_{des} \equiv \tau_h \cdot v_p + d_0 \end{aligned} \tag{4}$$

where v_p is the PV speed, d is the inter-vehicle distance, and d_{des} is the driver desired inter-vehicle distance, governed by the constant

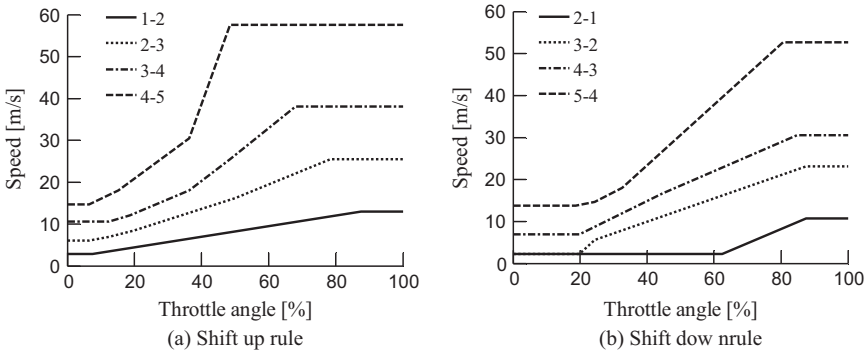

Fig. 4. Switching logic of automatic transmission.

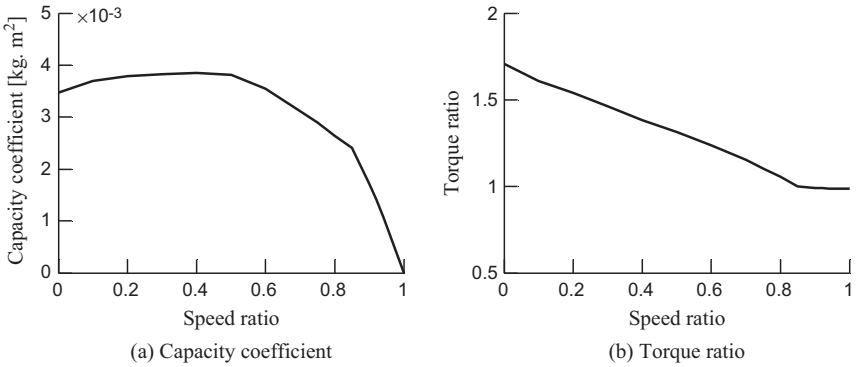

Fig. 5. Characteristics of torque converter.

Table 1
Parameters of vehicle dynamics.

Parameter	Unit	Value
M	kg	1747
i_0	–	3.86
r_w	m	0.30
C_A	kg/m	0.303
i_g	–	[3.62, 1.925, 1.285, 1.0, 0.667]

time headway (CTH) policy, τ_h is the headway time and d_0 is the offset [25]. For typical drivers of passenger cars, it is selected as τ_h = 1.5 s and d_0 = 5 m. For the inter-vehicle longitudinal dynamics, we have

$$\dot{d} = \Delta v \tag{5}$$

Collecting Eqs. (1), (4) and (5), we obtain the two-state space model by employing a new interim control variable u:

$$\begin{cases} \dot{\Delta d} = \Delta v - \tau_h a_p \\ \Delta \dot{v} = \varphi(v) + u + a_p + \frac{g_m}{\delta} \cdot \theta \end{cases} \qquad \varphi(v) \equiv \frac{1}{\delta M}\left(\frac{1}{2} C_A A \rho v^2 + M g_m f\right) \tag{6}$$

where a_p is the PV acceleration, $\varphi(v) \in \mathbb{C}$ is a nonlinear function of vehicle speed v, and u is the interim control variable, which has nonlinear relationship with T_t, defined below in Eq. (7)

$$u = \frac{i_g i_0 \eta_T}{M r_w} T_t \tag{7}$$

If considering u as the control input, Eq. (6) can be well regarded as a time-invariant model even though the gear is not fixed. Under the minimum sensor framework, the lack of accelerometer often weakens the accurate tracking of vehicle acceleration, which consequently leads to slow convergence speeds and large tracking errors. The TSM control law has good robustness, but its singularity

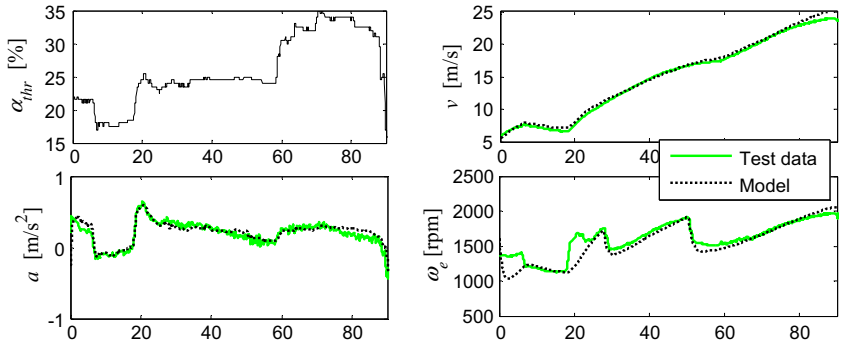

Fig. 6. Verification of model accuracy using car test data.

and chattering issues restrict its practical applications. Considering both the issues of singularity and chattering, a terminal sliding mode controller is proposed for Eq. (6):

$$u = \varphi(v) + \frac{\beta q}{p}\phi s + \frac{\beta q}{p}\Delta v^{2-p/q}\left(1 + \frac{g}{\alpha h}\Delta d^{g/h-1}\right) \tag{8}$$

where T_{tdes} is the desired turbine torque from the TSM controller. In Eq. (8), s is the sliding mode, defined as

$$s = \Delta d + \frac{1}{\alpha}\Delta d^{g/h} + \frac{1}{\beta}\Delta v^{p/q} \tag{9}$$

where $\alpha \in \mathbb{R}^+$, $\beta \in \mathbb{R}^+$, and $p, q, g, h \in N^+$ are odds, satisfying $1 < p/q < 2$ and $1 < p/q < g/h$. The associated reaching law is given by

$$\dot{s} = -\phi s \cdot \Delta v^{p/q-1} \tag{10}$$

where $\phi \in \mathbb{R}^+$. In the control law (8), the exponentials of Δv and Δd are positive, and thus there is no singularity issue. The exponential term of Δv in Eq. (8) contains a factor related to Δd, i.e. $\left(1 + \frac{g}{\alpha h}\Delta d^{g/h-1}\right)$. When the tracking errors are far away from equilibrium, this factor has a tendency to improve the convergence speed. As the state approaches the equilibrium point, this factor approximates 1 and Eq. (8) becomes similar to conventional TSM control. In addition, the control law in Eq. (8) is not directly connected to the engine inputs. The following inverse static equalities are needed to further compute desired engine torque T_{edes} and desired engine speed ω_{edes} for the engine:

$$\begin{aligned} T_{tdes} &= \frac{\delta M r_w}{i_g i_0 \eta_T} u \\ T_{edes} &= C_{TC}\left(\frac{r_w \cdot \omega_{edes}}{i_g i_0 v}\right)\omega_{edes}^2 \\ T_{tdes} &= K_{TC}\left(\frac{r_w \cdot \omega_{edes}}{i_g i_0 v}\right)T_{edes} \end{aligned} \tag{11}$$

Note that the inverse static equalities are derived by assuming that engine dynamics and the inertia of the flywheel are neglected. These assumptions naturally cause large errors in engine control. Therefore, a PID-based inner loop controller for the engine is used to compensate for the error in dynamic condition, as shown in Fig. 7. The inner loop controller has two PID controllers, and a forward compensator. The forward compensator is based on the inverse torque model of engine, i.e. the function $\alpha_{thrdes} = \text{MAP}^{-1}(T_{edes}, \omega_{edes})$ (Note that MAP^{-1} is the inverse function of MAP). Between gear shifts, the gear ratio i_g is fixed and Eq. (6) is a time-invariant model. When the gears are shifted, the state transition can be taken as the initial error of states. For normal driving conditions, frequent gear switching does not always occur because vehicle speed usually changes smoothly. Hence, any initial error will converge before the next gear switching since a long period exists between two shifts. This is particularly true for sparse traffic flows on city highways or inter-city expressways. The automated car-following controller is designed for FV to track PV in an accurate and robust manner.

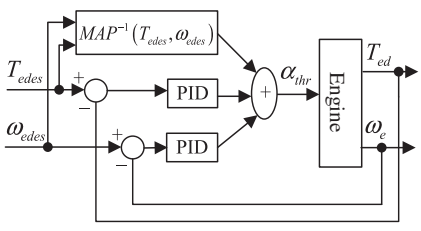

Fig. 7. Inner loop controller for engine.

4. Performance analysis of closed-loop control system

In this section, we further analyze the robustness of abovementioned controller under the minimum sensor framework. The analysis and proof will be first carried out for nominal condition, and then extend to a more realistic condition with both parameter variations and external disturbances. For nominal conditions, it is assumed that the vehicle is running on a flat road and the PV is running at a constant speed. Neglecting the unmodelled dynamics and parameter errors in Eq. (6), the nominal plant model becomes

$$\begin{cases} \Delta\dot{d} = \Delta v \\ \Delta\dot{v} = \varphi(v) + u \end{cases} \tag{12}$$

It is easy to know that $[\Delta d, \Delta v] = 0$ is the exclusive equilibrium point. In Section 4.1, we prove two theorems. Theorem 1 points out that the sliding plane (6) globally exists and any state starting from Eq. (9) converges to zeros at least asymptotically. Theorem 2 points out that from any initial position, the state will reach the sliding plane (6) asymptotically. Theorems 1 and 2 together show that Δd and Δv converge to zeros for nominal conditions. Section 4.2 then proves that, with the aforementioned controller, bounded external disturbances lead to bounded tracking errors in steady state. We start the analysis with a simple condition, i.e., $a_p = 0$ and $\theta \neq 0$, resulting in Theorem 3; Then we extend the results to more general uncertain condition, i.e., $a_p \neq 0$ and $\theta \neq 0$.

4.1. Stability analysis for nominal plant model

Theorem 1. *For the nominal model* Eq. (12), *any state* $x = [\Delta d, \Delta v]$ *starting from* Eq. (9), *i.e.* $x \in \{[\Delta d, \Delta v] | s = 0\}$, *converge to zeros in a finite time T.*

Proof. When $x \in \{[\Delta d, \Delta v] | s = 0\}$, we have

$$\dot{\Delta d}^{p/q} + \beta\Delta d + \frac{\beta}{\alpha}\Delta d^{g/h} = 0 \tag{13}$$

Define the Lyapunov function for the sliding mode

$$V(t) = 0.5 \cdot \Delta d^2 \tag{14}$$

Its derivative $V(t)/dt$ becomes

$$\dot{V}(t) = -\left(\beta\Delta d^{\frac{p+q}{q}} + \frac{\beta}{\alpha}\Delta d^{\frac{p}{q}+\frac{g}{h}}\right)^{q/p} \tag{15}$$

Thus $\dot{V}(t) < 0$ for any $[\Delta d, \Delta v] \neq 0$ considering $p, q, g, h \in N^+$ are odds, satisfying $1 < p/q < 2$ and $1 < p/q < g/h$. Therefore, the state is stable in the sliding mode, and the state at least asymptotically converges to zeros. □

Theorem 2. *For the nominal model* Eq. (12) *with the controller* Eq. (8), *the state from any initial point asymptotically reaches the sliding plane, i.e. the sliding mode globally exists.*

Proof. Define the Lyapunov function for the reaching mode

$$V(s) = 0.5 \cdot s^2 \tag{16}$$

Then,

$$\dot{V}(s) = s \cdot \dot{s} = -\phi s^2 \Delta v^{p/q-1} \tag{17}$$

Divide the $\Delta d - \Delta v$ phase plane into two regions

$$\begin{aligned} D &= \{x | \Delta d \neq 0,\ \Delta v \neq 0\} \\ \overline{D} &= \{x | \Delta d \neq 0,\ \Delta v = 0\} \end{aligned} \tag{18}$$

For any $x \in D$, $\dot{V}(s) < 0$. Hence, the sliding mode s asymptotically converges in D. Note that $\bar{D}$ is special case. To prove that s still converges in, $\bar{D}$ we substitute Eq. (8) into Eq. (12). Then, we can compute the gradient equation of state as

$$\frac{\Delta\dot{d}}{\Delta\dot{v}} = \frac{-\frac{\beta q}{p}\left[\phi s + \Delta v^{2-p/q}\left(1 + \frac{g}{\alpha h}\Delta d^{g/h-1}\right)\right]}{\Delta v} \tag{19}$$

Note that $p/q < 2$, and p, q, g, h are all odds. For $\Delta d > 0$ and $\Delta v = 0$, we have

$$\begin{aligned} &\frac{\Delta\dot{d}}{\Delta\dot{v}} = -\infty \\ &\Delta\dot{v} = -\frac{\beta q\phi}{p}\left[\Delta d + \frac{1}{\alpha}\Delta d^{g/h}\right] < 0 \end{aligned} \tag{20}$$

It is observed from Eq. (20) that the state cannot stay in $\bar{D}$ because $\Delta\dot{v} < 0$, and eventually it will enter D, in which the sliding mode s has been proved to asymptotically converge. Thus, the state from any initial position should reach the sliding plane asymptotically. □

4.2. Robust analysis for uncertain plant model

In reality, the model uncertainties, such as parametric errors, sensor noises, and external disturbances inevitably exist in an automated car-following system. In such cases, Δd and Δv will not converge to zero, but only to a neighborhood of equilibrium. For ground vehicles, the two dominating uncertainties are the road slope θ and the PV acceleration a_p. The road slope affects FV accelerating/decelerating abilities, leading to unpredictable tracking capabilities. The same arguments hold when the PV accelerates or decelerates.

Theorem 3. *Consider the uncertain model* Eq. (6) *with the controller (5), and assume that the PV runs at a constant speed, i.e., $a_p = 0$ and the road slope is bounded by $|\theta| < \kappa$ with $K \in \mathbb{R}^+$. Then the sliding mode s converges to a set Π defined by*

$$\Pi = \left\{\dot{s} \middle| |s| < \frac{pg_m\kappa}{\phi\beta q}\right\} \tag{21}$$

and the convergence speed is no less than the dynamics defined by

$$\dot{s}\cdot\mathrm{sgn}(s) = -\left(\phi|s| - \frac{pg_m\kappa}{\beta q}\right)\Delta v^{p/q-1} \tag{22}$$

Proof. Substituting Eq. (8) into Eq. (6), the dynamics of the sliding mode becomes

$$\begin{aligned} &\Delta\dot{d} = \Delta v - \tau_h a_p \\ &\Delta\dot{v} = -\frac{\beta q}{p}\left[\phi s + \Delta v^{2-p/q}\left(1 + \frac{g}{\alpha h}\Delta d^{g/h-1}\right)\right] \end{aligned} \tag{23}$$

Differentiating Eq. (9), we have

$$\dot{s} = \left(1 + \frac{g}{\alpha h}\Delta d^{g/h-1}\right)\Delta\dot{d} + \frac{p}{\beta q}\Delta v^{p/q-1}\Delta\dot{v} \tag{24}$$

Substituting Eq. (23) into Eq. (24) and considering that $a_p = 0$, we have

$$\dot{s} = -\left(\phi s + \frac{pg}{\beta q}\cdot\frac{g_m}{\delta}\cdot\theta\right)\Delta v^{p/q-1} \tag{25}$$

For any types of vehicles, δ satisfies (see Eq. (2))

$$\delta > 1 \tag{26}$$

Considering $|\theta| < \kappa$ and the sign of S, we have

$$\dot{s}\cdot\mathrm{sgn}(s) < -\left(\phi|s| - \frac{pg_m\kappa}{\beta q}\right)\Delta v^{p/q-1} \tag{27}$$

According to Eq. (27), it is found that the sliding mode s converges when outside of set Π, and the convergence speed is no less than Eq. (22). The convergence of sliding mode s is uncertain when inside of set Π. But at least we know that the sliding mode stays inside set Π once it reaches Π. □

For a general condition, where both $a_p \neq 0$ and $\theta \neq 0$ hold, an equivalent theorem is not easy to establish. For the sake of simplicity, we assume that both a_p and θ are constant during driving. The derivative of state pair $(\Delta d, \Delta v)$ must converge to zero in the steady state condition.

$$\begin{aligned} &\Delta\dot{d} = 0 \\ &\Delta\dot{v} = 0 \end{aligned} \tag{28}$$

Substituting Eq. (28) into Eq. (23), we have

$$\Delta v = \tau_h a_p, \tag{29}$$

$$a_p + \frac{g_m}{\delta}\theta = \frac{\beta q}{p}\left[\phi s + \Delta v^{2-p/q}\left(1 + \frac{g}{\alpha h}\Delta d^{g/h-1}\right)\right] \tag{30}$$

The Eq. (29) describes the relationship between Δv and a_p in steady state situation. Substituting Eqs. (29) and (9) into Eq. (30), we have

$$\begin{aligned} a_p + \frac{g_m}{\delta}\theta = \frac{\beta q}{p}\phi\left(\Delta d + \frac{1}{\alpha}\Delta d^{g/h} + \frac{1}{\beta}(\tau_h a_p)^{p/q}\right) \\ + \frac{\beta q}{p}(\tau_h a_p)^{2-p/q}\left(1 + \frac{g}{\alpha h}\Delta d^{g/h-1}\right) \end{aligned} \tag{31}$$

The Eq. (31) depicts the relationship between Δd and a_p, θ in steady state condition. This means that the closeness of Δd to zeros is dominated by a_p and θ (as well as selected parameters in controller design). Fig. 8 numerically illustrates this relationship. Fig. 8(a) is obtained with controller parameters shown in Table 2 in Section 6.1, and Fig. 8(b)–(d) have some parametric variations on β, ϕ, and τ_h, respectively. We observe that the steady state of Δd depends on a_p and θ, as well as designed controller parameters. A desirable convergence can be obtained by properly selecting control parameters.

For any PV, due to the limited engine power, a_p is bounded. The road slope θ is also bounded for real road conditions. Thus both Δd and Δv converge to a neighborhood of equilibrium constrained by Eqs. (31) and (29), respectively. In reality, vehicle speed fluctuates on waved roads, and both a_p and θ are not constant. The same conclusions on tracking errors almost hold here because of relatively slow variations on a_p and θ in normal traffic flows.

5. Simulation results and field tests

In this section, we demonstrate the effectiveness of above-design controller via simulations and field tests. The testing platform is chosen as the same at that of the passenger car introduced in Section 3.1. The passenger car has a powertrain including internal combustion engine, torque converter, automatic transmission, final gear, half axes, and four wheels. The key parameters of vehicle longitudinal dynamics are listed in Table 1. The MMW (Mili-Meter Wave) radar is used to detect targets, e.g., PVs or obstacles. No IMU is installed, which satisfies the requirement of the minimum sensor framework.

5.1. Simulation with CarSim and Simulink

CarSim is commonly used for the simulation of vehicle longitudinal dynamics. It can provide accurate and realistic predictions of vehicle inner states. CarSim is an integrated software package that can run co-simulations with other software, e.g., Matlab/Simulink. Combining CarSim and Simulink, we developed a hybrid simulation

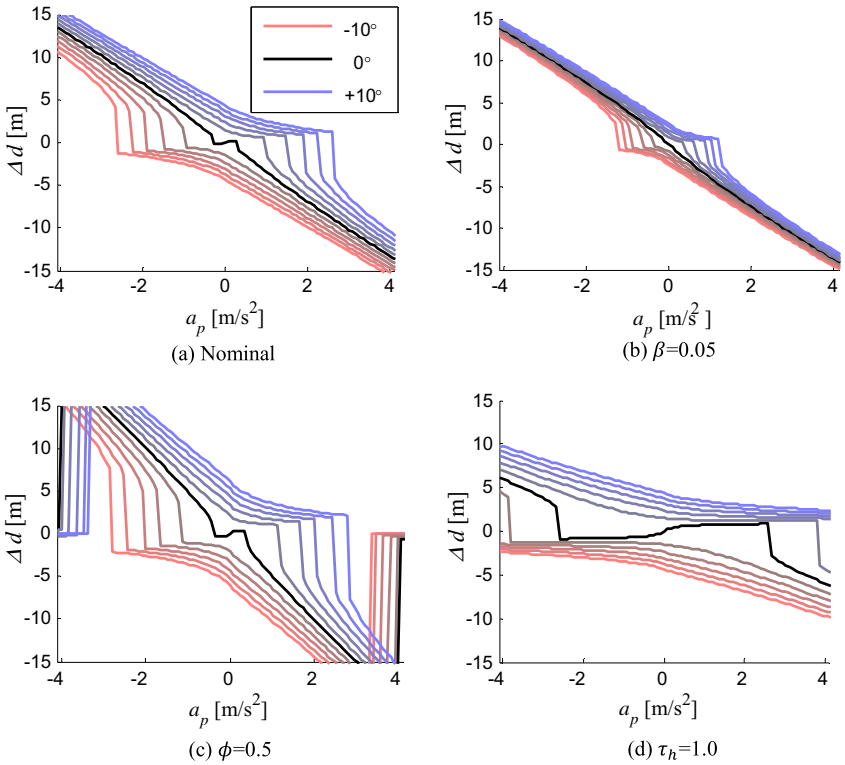

Fig. 8. Distance error in steady state condition under constant disturbances. (In each sub-figure, each line represents a road slope angle, ranging from −10° to 10° with interval 2°.)

Table 2
Controller parameters.

$\alpha = 0.1$	$\beta = 0.1$	$p = 15$	$q = 13$
$g = 17$	$h = 11$	$\phi = 0.1$	$\eta = 2$
$k_v = 0.5$	$k_d = 0.2$		

model, shown in Fig. 9. The vehicle longitudinal dynamics is simulated by CarSim and other components, e.g., controllers and driving scenarios, are implemented in Simulink.

The involved automated car-following controllers in simulations include a linear car-following controller (shorted as LCF), a conventional TSM controller (shorted as c-TSM), and the newly proposed TSM controller (shortened to n-TSM). The n-TSM controller is designed based on the control law given in (8), in which both singularity and chattering issues are avoided, and desirable robust performance is also ensured. The other two controllers are designed for the purpose of comparison. The linear car-following (LCF) controller is designed based on linear microscopic traffic flow models [27]. The reason to select a linear car-following controller is that this model has good mimic of the car-following behavior of human drivers, and is often taken as a simplified replacement for human drivers in many studies, e.g. mixed traffic flow, co-pilot driving, etc. The feedback law of LCF is given by

$$u = k_v \Delta v + k_d \Delta d \tag{32}$$

The c-TSM is designed based on conventional terminal sliding mode control theory, as shown in [22,23]. In conventional TSM, a nonsingular sliding function is employed, and a reaching law with switching term is included. The feedback law of c-TSM is given by

$$u = \varphi(v) + \frac{\beta q}{p} \Delta v^{1-p/q} (\phi s + \eta \mathrm{sgn}(s) + \Delta v) \tag{33}$$

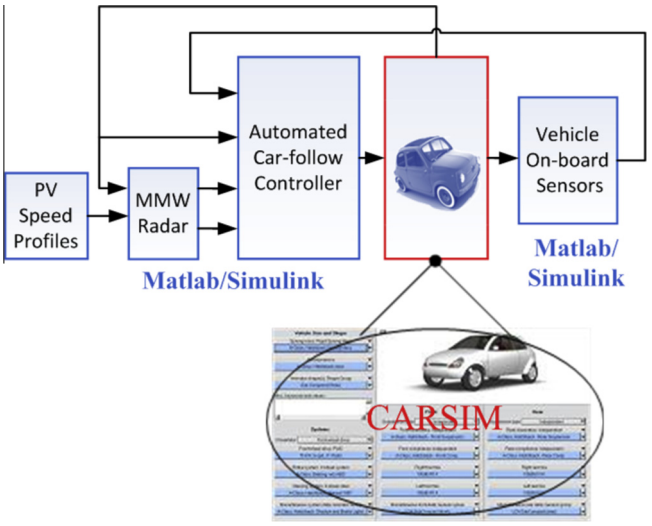

Fig. 9. Hybrid simulation model framework.

Both Eqs. (32) and (33) use the interim symbol u, which has identical definition as in Eq. (8). The parameters used by three controllers are shown in Table 2. The c-TSM controller (2) and n-TSM controller (8) share almost the same set of parameters, and the LCF controller (1) uses a set of parameters close to typical human drivers [27]. Three traffic scenarios are considered in the simulation: one on a flat road ($\theta = 0°$) and the other two on a road with slope ($\theta = 2°$ and $\theta = 4°$). In all three scenarios, PV runs at the same speed profiles. The PV first runs at the constant speed of 10 m/s and then starts to accelerate at a given acceleration profile, as shown in Fig. 10. Fig. 11 shows the simulations results when $\theta = 0°$, with

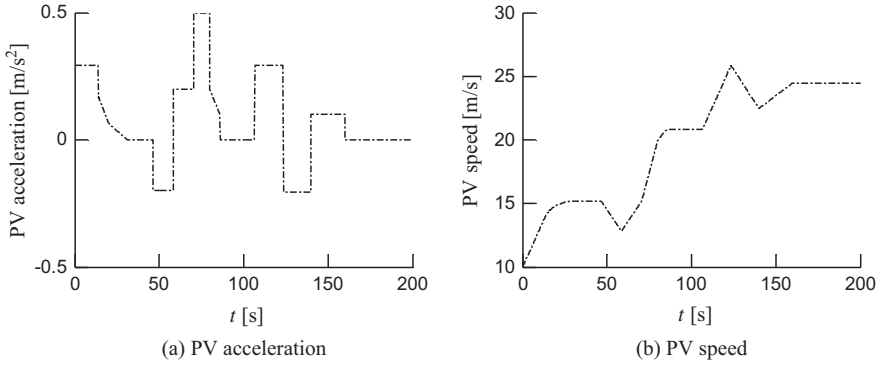

Fig. 10. Acceleration and speed profiles of preceding vehicle.

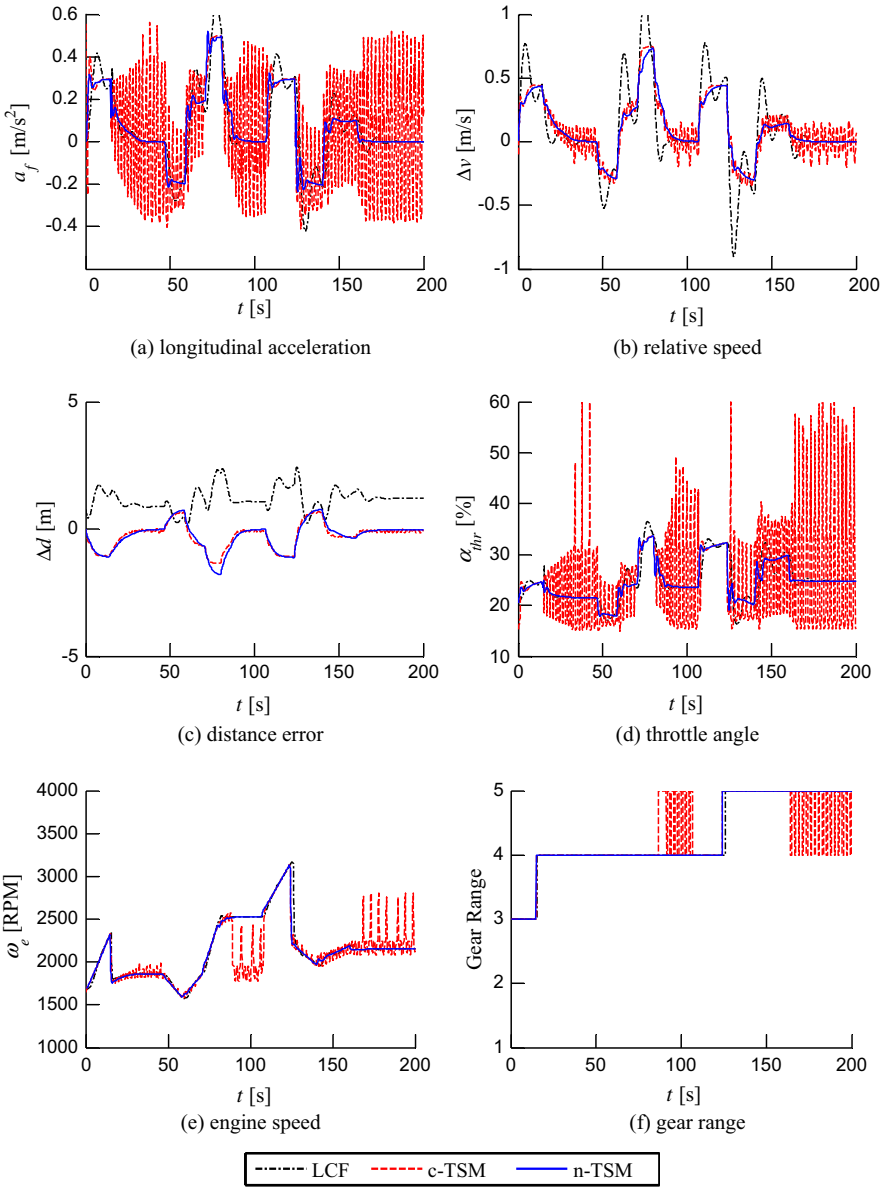

Fig. 11. Simulation results in accelerating scenario one the flat road ($\theta = 0°$).

(a) longitudinal acceleration, (b) relative speed, (c) distance error, (d) throttle angle, (e) engine speed, and (f) gear range. Figs. 12 and 13 show the simulation results when $\theta = 2°$ and $\theta = 4°$, respectively.

In Fig. 11, two successive vehicles run on the flat road ($\theta = 0°$). As illustrated in Fig. 11, all three controllers are stable and both Δd and Δv converge. The LCF controller generates a continuous profile of throttle angle, subsequently leading to smoothly

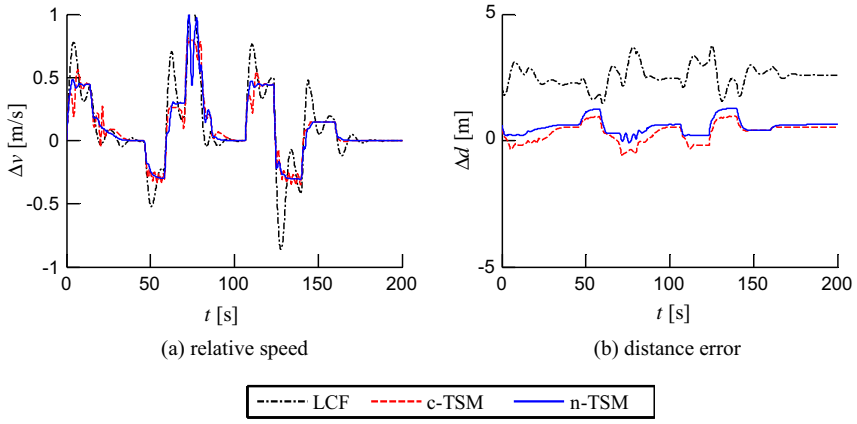

Fig. 12. Simulation results in accelerating scenario on the slope ($\theta = 2^{\circ}$).

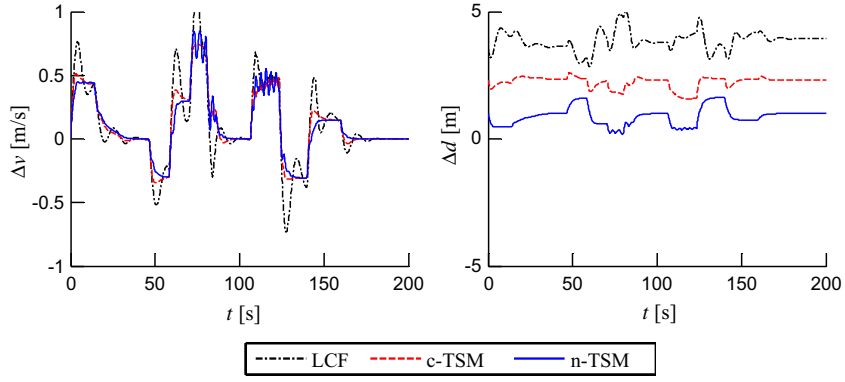

Fig. 13. Simulation results in accelerating scenario on the slope ($\theta = 4°$).

changing acceleration, speed, and distance. Some overshooting problem exists in its relative speed profile and it also has larger distance errors than others. The c-TSM controller has a similar performance as the n-TSM controller. However, as shown in Fig. 11(d), the c-TSM controller has inevitable chartering issue, which is caused by the switching term in its control law. We observe that the n-TSM controller overcomes this chattering issue. The tracking performance of c-TSM and n-TSM are similar at the flat road ($\theta = 0°$). When vehicles run on the slope road, n-TSM begins to exhibit better performance than both c-TSM and LCF. As shown in Figs. 12 and 13, all three controllers are still stable, but have larger tracking errors than those on the flat road (one main reason is that there is no lower level controller for acceleration tracking due to missing acceleration information). The LCF controller has the largest tracking errors in terms of both Δd and Δv. The c-TSM also leads to a larger distance error, but is better than LCF's. This is consistent with the fact that the sliding mode control method is more robust than the linear one. Among them, the n-TSM controller performs the best in robust performance, particularly on effectively depressing the amplitude of tracking errors caused by road slope.

Fig. 14 summarizes the robust performance of the three controllers. Fig. 14(a) shows the absolute mean of relative speed is almost independent of the road slope in the three controllers. This is mainly because of the fact that the control on distance error actually has the "integrator" effect on the relative speed, and eliminates the steady state error of relative speed. However, regarding

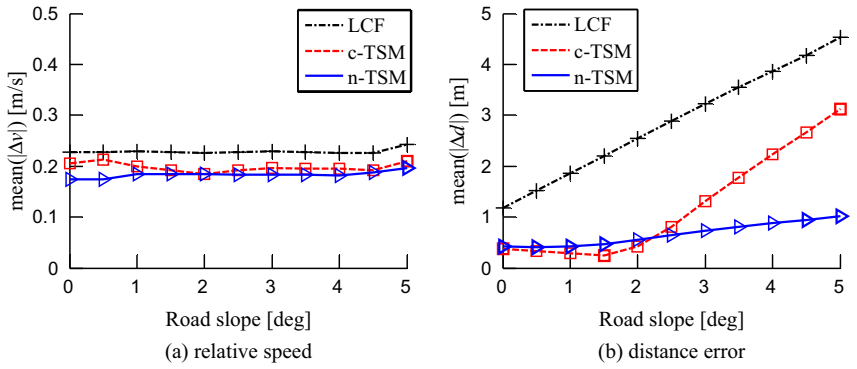

Fig. 14. Robustness test of controllers to road slope.

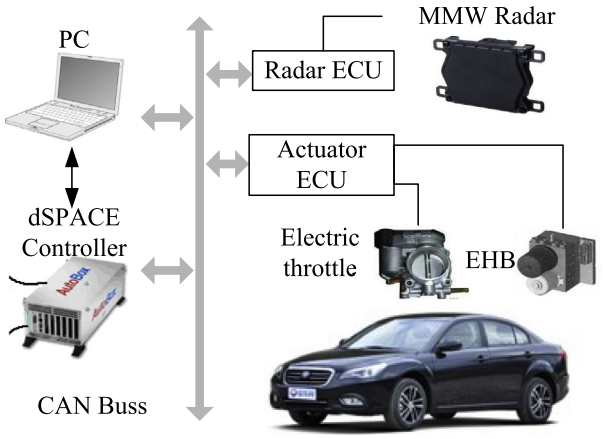

Fig. 15. Configuration of test platform.

the absolute mean of distance error, LCF almost linearly increases with road slope; the c-TSM first slowly drops and then quickly increases with road slope. The n-TSM controller performs the best which significantly depresses the increase of distance error with road slope.

5.2. Field test results

The n-TSM controller is further validated through the field tests with a passenger car. The configuration of the test platform is shown in Fig. 15. The test vehicle is a passenger car, with 2.0L gasoline engine, 5-speed automated transmission, and hydraulic braking system. Fig. 15 shows the photos of the test car and experimental scenarios. The passenger car for the test is equipped with a dSPACE prototyping controller, an MMW radar, an electric throttle, an electro-hydraulic brake (EBH) actuator, as well as power suppliers. The dSPACE controller is used to implement the n-TSM control algorithm and other necessary algorithms such a radar signal processing algorithm, a human–machine interface, etc. The engine is regulated by an electronic throttle control while the braking system is controlled by Electro-Hydraulic Brake (EHB). The inter-vehicle information is detected by the MMW radar. Sensors, controllers, and actuators share information using a CAN bus, which also connects to the data center of the passenger car. The collected information from CAN bus comes from engine ECU, transmission ECU, ABS ECU. The MMW radar is also connected to the CAN bus, and such information as inter-vehicle distance and relative speed to the target is sent periodically to CAN. The CAN bus uses the following protocols which include: (1) SAE1939 standard with baud rate as 500bits/s; (2) The senders have different sampling frequency, ranging from 1 m/s to 100 m/s, depending on the importance of information; (3) The data frame follows the Motorola format, with length as 11 bits. For the sake of real-time implementation, all data frames related to control commands are to the highest priority and fixed period 100 m/s (see Fig. 16).

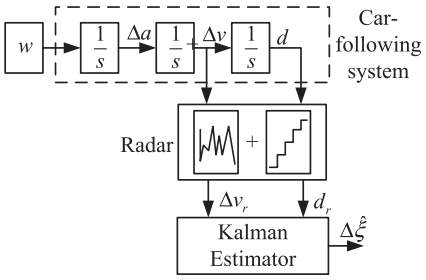

Fig. 17. State space model structure to design Kalman filter.

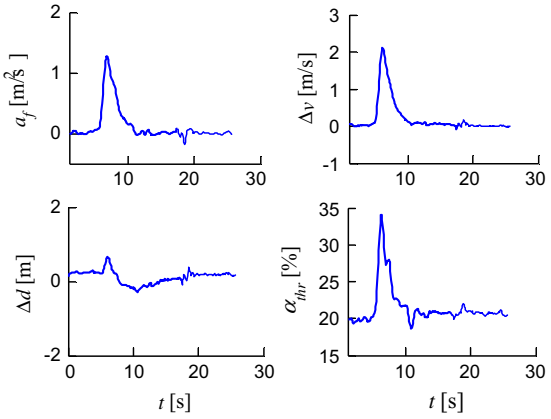

Fig. 18. Test results in cut-in scenario.

In addition, the radar output is not directly used in the dSPACE controller. The MMW radar is used to measure the inter-vehicle distance and relative speed between two vehicles. The relative speed and distance error is filtered via a Kalman filter, which is based on a state space model with four states, which include inter-vehicle distance (d), relative speed (Δv), relative acceleration (Δa) and relative jerk (w). The state space model structure is shown in Fig. 17. The relative jerk (w) is assumed to be band-limited white noise. Fig. 17 shows the structure of state space model for Kalman filter design.

In Fig. 18, a cut-in scenario is considered in the field test. The FV first runs at a speed of around 5 m/s. At 5 s, the PV cuts in from adjacent lane with higher speed 8.06 m/s and the initial distance ahead of FV around 14 m. In Fig. 19, an accelerating scenario is considered in the field test. The PV first runs at the approximate speed of 5 m/s, and starts to accelerate at approximately 0.5 m/s^2 until

Fig. 16. Photos of test car and experimental scenarios.

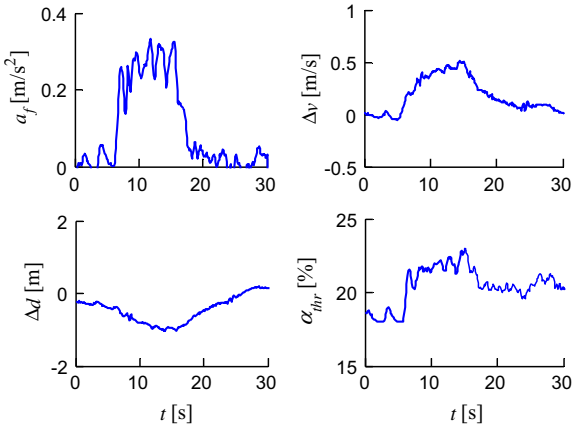

Fig. 19. Test results in accelerating scenarios.

the speed reaches 7.8 m/s. In both scenarios, the FV is controlled by the n-TSM method. It is found that the n-TSM controller successfully fulfills an automated car-following function without reliance on any information of longitudinal acceleration.

6. Conclusions

The concept of minimum sensor helps reduce the number of sensors in vehicle automation. This framework is a promising approach to decrease hardware costs of autonomous vehicles without significantly losing control performance and system reliability. This paper presents a nonsingular and fast terminal sliding mode controller for automated car-following system under the minimum sensor framework. A nonsingular fast terminal function is proposed to improve the convergence speed of sliding mode, and a novel terminal attractor is adopted as the reaching law. Such a controller has high robustness to model uncertainties and external disturbances, without issues of singularity and chattering that accompany with many other conventional sliding mode controllers. This high robustness helps to reduce the tracking errors in automated car-following systems even without reliance on the information of longitudinal acceleration. Under the minimum sensor framework, the stability under nominal condition is also proved and analyzed. It is also proved that the newly designed controller is able to generate bounded stability under some mild assumptions on leading vehicle acceleration and road slope. We demonstrate the effectiveness of the designed controller and its robustness to external disturbances via computer simulations and field tests.

Acknowledgements

The research work was partially supported by NSF China Foundation under Grant 51205228. The research is also partially supported by Tsinghua University Initiative Scientific Research Program under Grant 20121088076. The authors gratefully acknowledge Prof. Jianqiang Wang and Dr. Feng Gao in Tsinghua University for his suggestions on controller designs and field tests.

References

[1] Khayyam H, Nahavandi S, Davis S. Adaptive cruise control look-ahead system for energy management of vehicles. Exp Syst Appl 2012;39(3):3874–85.
[2] Ioannou P, Chien C. Autonomous intelligent cruise control. IEEE Trans Vehicul Tech 1993;42(4):657–72.
[3] Wang R, Zhang H, Wang J. Linear parameter-varying controller design for four-wheel independently actuated electric ground vehicles with active steering systems. IEEE Trans Control Syst Tech 2014;22(4):1281–96.
[4] Kim C, Langari R. Development of an autonomous vehicle highway merging strategy. Intl J Vehicle Des 2012;60(3–4):350–68.
[5] Swaroop D, Hedrick JK, Choi SB. Direct adaptive longitudinal control of vehicle platoon. IEEE Trans Vehicular Tech 2001;50(1):150–61.
[6] Ferrara A, Pisu P. Minimum sensor second-order sliding mode longitudinal control of passenger vehicles. IEEE Trans Intell Transp Syst 2004;5(1):20–32.
[7] Yi K, Kwon Y. Vehicle-to-vehicle distance and speed control using an electronic-vacuum booster. JSAE Rev 2001;22(4):403–12.
[8] Li S, Li K, Rajamani R, Wang J. Model predictive multi-objective vehicular adaptive cruise control. IEEE Trans Control Syst Tech 2011;19(3):556–66.
[9] Eben Li S, Peng H. Optimal strategies to minimize fuel consumption of passenger cars during car-following scenarios. iMech-E Part D: J Automob Eng 2012;226(3):419–29.
[10] Fritz A, Schiehlen W. Automatic cruise control of a mechatronic ally steered vehicle convoy. Vehicle Syst Dynam 1999;32(4–5):331–44.
[11] Corona D, De Schutter B. Adaptive cruise control for a SMART car: a comparison benchmark for MPC-PWA control methods. IEEE Trans Control Syst Tech 2008;16(2):365–72.
[12] Hebbale K, Ghoneim Y. A speed and acceleration estimation algorithm for powertrain control. In: American Control Conf, Boston, MA, USA; 1991. p. 415–20.
[13] Venkataraman S, Gulati S. Terminal sliding modes: a new approach to nonlinear control synthesis. In: The 5th Int Conf Adv Robot, Pisa, Italy; 1991. p. 443–8.
[14] Man Z, Yu X. Terminal sliding mode control of MIMO linear systems. IEEE Trans Circ Syst I: Fundam Theory Appl 1997;44(11):1065–70.
[15] Wu Y, Yu X, Man Z. Terminal sliding mode control design for uncertain dynamic systems. Syst Control Lett 1998;34(5):281–7.
[16] Man Z, Paplinski P, Wu R. A robust MIMO terminal sliding mode control scheme for rigid robotic manipulators. IEEE Trans Autom Control 1994;39(12):2464–9.
[17] Yu X, Man Z, Wu Y. Terminal sliding modes with fast transient performance. In: Proceedings of the 36th IEEE conference on decision and control, vol. 2; 1997. p. 962–3.
[18] Yu S, Guo G, Man Z, Du J. Global fast terminal sliding mode control for robotic manipulators. Int J Model Ident Control 2006;1(1):72–9.
[19] Yu S, Yu X, Man Z. Robust global terminal sliding mode control of SISO nonlinear uncertain systems. In: Proceedings of the 39th IEEE conference on decision and control, vol. 3; 2000. p. 2198–203.
[20] Yu X, Man Z. Fast terminal sliding-mode control design for nonlinear dynamical systems. IEEE Trans Circ Syst I: Fundam Theory Appl 2002;49(2):261–4.
[21] Feng Y, Bao S, Yu X. Design method of non-singular terminal sliding mode control systems. Control Decis 2002;17(2):194–8.
[22] Feng Y, Yu X, Man Z. Non-singular terminal sliding mode control of rigid manipulators. Automatica 2002;38(12):2159–67.
[23] Feng Y, Yu X, Man Z. Non-singular terminal sliding mode control and its application for robot manipulators. In: IEEE international symposium on circuits and systems, the 2001 ISCAS, vol. 3; 2001. p. 545–8.
[24] Cho D, Hedrick J. Automotive powertrain modeling for control. J Dynam Syst, Measur Control 1989;111(4):568–76.
[25] Eben Li S, Li K, Wang J. Economy oriented vehicle adaptive cruise control with coordinating multiple objectives function. Vehicle Syst Dynam 2013;51(1):1–17.
[26] Nouveliere L, Mammar S. Experimental vehicle longitudinal control using a second order sliding mode technique. Control Eng Pract 2007;15(8):943–54.
[27] Gipps P. A behavioral car-following model for computer simulation. Transp Res Part B: Methodol 1981;15(2):105–11.